Universiteit
Antwerpen

This item is the archived peer-reviewed author-version of:

Tuning the quantum phase transition of an ultrathin magnetic topological insulator

Reference:
Shafiei Mohammad, Fazileh Farhad, Peeters François, Milošević Milorad.- Tuning the quantum phase transition of an ultrathin magnetic topological insulator
Physical review materials / American Physical Society - ISSN 2475-9953 - 8:7(2024), 074201
Full text (Publisher's DOI): https://doi.org/10.1103/PHYSREVMATERIALS.8.074201
To cite this reference: https://hdl.handle.net/10067/2075980151162165141

uantwerpen.be
Institutional repository IRUA

Tuning the quantum phase transition of an ultra-thin magnetic topological insulator

Mohammad Shafiei,[1,2] Farhad Fazileh,[2] François M. Peeters,[3,4,1] and Milorad V. Milošević[1,5,*]

[1] *Department of Physics, University of Antwerp, Groenenborgerlaan 171, B-2020 Antwerp, Belgium*
[2] *Department of Physics, Isfahan University of Technology, Isfahan 84156-83111, Iran*
[3] *Nanjing University of Information Science and Technology, Nanjing 210044, China*
[4] *Departamento de Física, Universidade Federal do Ceará, 60455-760 Fortaleza, Ceará, Brazil*
[5] *NANOlab Center of Excellence, University of Antwerp, B-2020 Antwerp, Belgium*

(Dated: August 29, 2024)

We explore the effect of thickness, magnetization direction, strain, and gating on the topological quantum phase transition of a thin-film magnetic topological insulator. Reducing the film thickness to the ultra-thin regime couples the edge states on the two surfaces, opening a gap known as the hybridization gap, and causing a phase transition from a topological insulator to a normal insulator (NI). An out-of-plane/in-plane magnetization of size proportional to the hybridization gap triggers a phase transition from a normal insulator state to a quantum anomalous Hall (QAH)/semimetal state. A magnetization tilt by angle θ from the out-of-plane axis, influences the topological phase transition, in a way that for sufficiently large θ, no phase transition from NI to QAH can be observed regardless of the sample thickness or magnetization, and for θ close to $\pi/2$ the system transits to a semi-metal phase. Furthermore, we demonstrate that compressive/tensile strain can be used to decrease/increase the magnetization threshold for the topological phase transition. Finally, we reveal the effect of a vertical potential acting on the film, be it due to the substrate or applied gating, which breaks inversion symmetry and raises the magnetization threshold for the transition from NI to QAH state.

I. INTRODUCTION

One of the most fundamental aspects of studying topological phases of matter in condensed matter physics are topological quantum phase transitions, which may occur when material compositions or sample dimensions change[1–3]. This has prompted several fundamental studies[4,5] which divided materials into two groups depending on their symmetries: the ones with spontaneously broken symmetry and the ones exhibiting a topological phase of matter. In the spontaneously broken symmetry case, distinct phases with constant order parameters, such as ferromagnetism and ferroelectricity, emerge. Topological phases of matter, like topological insulators, Weyl semimetals, and Chern insulators, are characterized by invariants, such as Chern number and the $\mathbb{Z}_2$ invariant, that are insensitive to continuous changes of parameters[5].

Theoretical predictions of topological phases motivated the experimentalists to identify these states, leading to the discovery of the quantum Hall effect (QHE) phases[6]. For example, Haldane proposed the emergence of the quantum anomalous Hall states about four decades ago for a honeycomb lattice[7], and after identifying TIs experimentally, QAH states were observed in V-doped and Cr-doped $(Bi,Sb)_2Te_3$[8]. The discovery of the QHE in a two-dimensional electron system with an external magnetic field revealed the topology of the band in the Brillouin zone[5]. Once a material is in a topological phase, its intrinsic properties cannot be affected by continuous variation of its parameters, nor can a local order parameter describe the phase[9,10]. In general, independent of the details, the phase transition is characterized by its critical behavior which depends on the dimension and symmetries of the system.

After the discovery of topological insulators (TIs) in two-dimensional systems, the three-dimensional TIs were introduced, first theoretically[11] and then experimentally[12], in $Bi_{1-x}Sb_x$ alloys with $0.09 < x < 0.23$. However, surface states in these alloys cut the Fermi level, rendering them unsuitable for the investigation of surface state properties[12]. Subsequently, semiconductors of the Bi_2Se_3 family were investigated, becoming the most well-known three-dimensional TI due to their unique yet accessible surface states[11,13,14]. Retaining surface state conduction in the presence of the insulating bulk and defects poses a number of challenges. In order to overcome these difficulties, it is necessary to develop TI thin films.

From an electronic standpoint, bulk conduction and imperfections pose obstacles to surface state conduction in 3D TIs. By enhancing material synthesis techniques and reducing bulk carrier density[15], the creation of thin-film TI is a way to overcome these obstacles[16,17]. Several techniques, including co-evaporation, electrochemical deposition, and molecular beam epitaxy (MBE), are readily employed to produce such thin films, including the Bi_2Se_3 ones[18–20]. The molecular beam epitaxy (MBE) approach is often used to grow thin-film TI since it enables the synthesis of TI with thicknesses comparable to atomic layers and high doping control for the creation of TI-heterostructures[20]. In the ultra-thin film regime however, the wave functions of the surface states overlap, the surface states become gapped (exhibit the so-called hybridization gap), and the TI film turns into a normal insulator[21].

Independent studies on spontaneously broken symmetry phases and topological phases resulted in the ideas to induce the overlap of these phases in order to generate intriguing novel quantum phenomena. For example, mag-

netic order can be imparted to TIs by an applied magnetic field, doping them with magnetic elements, or positioning them near magnetic materials[22]. That in turn may cause the collapse of time-reversal symmetry (TRS), and instigate fascinating phenomena such as the QAH state and the topological magnetoelectric effect. Without an external magnetic field and with high carrier mobility, the QAH effect is widely recognized as a suitable platform for creating topological states of matter and topological devices[23]. Magnetization applied to TI may have different orientations in space, and if their magnetic order is out-of-plane, QAH states may develop[22]. The exchange coupling between the localized spin and the z-component of the Dirac electron's spin produces a gap in the surface states, which ARPES and spectroscopic imaging have experimentally verified[24,25].

The unique band structure of Bi_2Se_3 enables ferromagnetism in bulk states, and the introduction of magnetic impurities into TI leads to the formation of ferromagnetic coupling through significant van Vleck susceptibility in the gapped states[26], where the Fermi energy is situated[27]. To properly detect QAH in magnetic TI, several conditions must be fulfilled. First, the film must exhibit initial long-range ferromagnetic order, and the easy magnetization axis has to be perpendicular to the film's plane. Second, the film thickness requires to permit the localization of conduction electrons, which is attainable for thin films. However, if the TI thickness is too narrow and the ferromagnetic exchange gap is smaller than the hybridization gap, QAH will not appear. Lastly, the Fermi energy must reside inside the surface state gap generated by magnetization[28,29].

In this work we focus on magnetic TI thin films, in which magnetization and topological properties coexist. Such materials have potential applications in next-generation electronic devices such as low-energy spintronics, dissipationless topological electronic devices, switches and transistor devices, and topological quantum computing. Magnetic proximity and magnetic doping are the most common techniques for magnetizing TIs[30–32]. In this paper, we investigate the quantum topological phase transitions in such a magnetic TI in its ultra-thin limit, where the combination of a spontaneously broken symmetry phase and a topological phase will lead to novel quantum phenomena, highly sensitive to sample thickness, magnetization, strain, and gating. Our findings will serve as a useful guide for experimental control of the possible phases in thin-film topological insulators. One should note that the tight-binding model used in this study goes beyond previous models, by including the structural symmetries of the system under study. Furthermore, Ref. 33 introduces a real-space tight-binding model by calculating Slater-Koster coefficients for Bi_2Se_3. However, our model is more advanced because its parameters are obtained from fitting the experimental data, resulting in findings that closely match experimental results, particularly regarding the size of the hybridization gap and the localization of the surface states.

The paper is organized as follows. Section II presents our tight-binding Hamiltonian for Bi_2Se_3 films, and shows how magnetic exchange is included in the theoretical model for magnetic TIs. Subsequently the main results are shown in Sec. III, starting from the effect of sample thickness, magnetization and its direction on the topological quantum phase transitions. We determine the threshold tilt angle of magnetization with respect to the film plane for the appearance of topological transition in the ultra-thin film regime. We further show how strain modifies the magnetization threshold for the phase transition, and discuss the effect of an added vertical potential - that mimics the effect of a substrate and/or external gating field. Section IV summarizes our findings.

II. THEORETICAL FRAMEWORK

Elements in Bi_2Se_3 family (V_2VI_3 compounds) have a rhombohedral crystal structure with a D^5_{3d} ($R\bar{3}m$) symmetry group and five atoms per unit cell. Additionally, the structure can be viewed as a hexagonal primitive cell with five Se-Bi-Se-Bi-Se atomic layers, often known as a quintuple layer (QL) as shown in Fig. 1(b). The binding between Bi-Se atoms within each QL is covalent. In contrast, the link between QLs is weaker and of van der Waals type, resulting in the formation of a van der Waals gap and inducing anisotropy[20]. The Γ point of these compounds has a Dirac cone, and the bulk gap for Bi_2Se_3 is approximately 300 meV[34]. Given the existence of inversion symmetry, the $\mathbb{Z}_2$ invariant can be determined using the wave function's parity[13,34,35]. Surface states have such a strong spin-orbit coupling that spin Dirac fermions are locked to their momentum without backscattering. Angle-resolved photoemission spectroscopy (ARPES) has experimentally demonstrated the occurrence of these surface states[36].

In the Bi_2Se_3 family, the outermost shell of the electron configuration contains p orbitals. Therefore, we consider only p orbitals and ignored the other. Since we are dealing with five atoms inside each QL and taking into account the p orbitals only (p_x, p_y, and p_z), we are dealing with a total of 15 orbitals[13]. However, when we take into account the hybridization between atomic orbitals, the formation of bonding and antibonding states, crystal field splitting, and spin-orbit coupling, the Hamiltonian basis can be considered as $\left|P1^+_-, 1/2\right\rangle, -i\left|P2^-_+, 1/2\right\rangle, \left|P1^+_-, -1/2\right\rangle, i\left|P2^-_+, -1/2\right\rangle$. The upper sign is assigned to the inversion eigenvalue and 1/2 to the total angular momentum[13,34]. We consider the following tight-binding Hamiltonian for Bi_2Se_3 in real space, as proposed in Ref. 37:

$$H = \Sigma_i c_i^\dagger E_{on} c_i + \Sigma_{i,\alpha}(c_i^\dagger T_\alpha c_{i+\alpha} + H.c). \tag{1}$$

The hopping parameters of this Hamiltonian are 4×4 matrices:

$$E_{on} = (E_0 - 2\Sigma_\alpha B_\alpha)\sigma_z \otimes \sigma_0, \tag{2}$$

and

$$T_\alpha = C_\alpha \sigma_0 \otimes \sigma_0 + B_\alpha \sigma_z \otimes \sigma_0 - i(\frac{A_\alpha}{2})\sigma_x \otimes \sigma \cdot \mathbf{n}_\alpha, \quad (3)$$

where σ_i are Pauli matrices, and E_{on} and T_α stand for onsite energy and hopping parameters between unit cells, respectively. n_α (α =1, 2, 3 or 4) represent the lattice vectors, while T_α stands for the hopping parameters in the direction of these vectors. Indices α = 1, 2, and 3 denote quantities within the x-y plane. By fitting the band structure of this Hamiltonian with DFT data and considering particle-hole symmetry in the system without losing generality (C_α=0), the parameters in this Hamiltonian are $A_\parallel$=0.5 eV, A_z=0.44 eV, E_0=0.28 eV, and $B_\parallel$=B_z=0.25 eV. Once any magnetization is added in a TI, the surface electrons interact with the magnetization through exchange interaction, which is represented in the Hamiltonian through the term:

$$H_{ex} = M_i \sigma_i \otimes \sigma_0, \quad (i = x, y, z), \quad (4)$$

Transport calculations are performed utilizing the Landauer-Büttiker formalism and considering a four-terminal sample, where conductance (G) is represented in terms of the transmission coefficient between leads i and j as follows[5,38]:

$$T_{ij} = \mathrm{tr}[\Gamma_i G_{ij} \Gamma_j G_{ij}^\dagger], \quad (5)$$

G_{ij} represents Green's function and Γ_i indicates the coupling between the leads and the sample, which is defined as $\Gamma_i = i[\Sigma_i - \Sigma_i^\dagger]$ in terms of self-energy Σ_i.

In previous theoretical works[22,39], modeling the system as a surface of a TI was a common approach. However, this method did not consider some essential aspects of TIs in the thin-film regime, such as the overlap of the surface wave functions. Moreover, the in-plane magnetization component has a different impact in the thin-film regime compared to the thick-film regime, and it cannot be eliminated by a gauge transformation, therefore, it should be properly addressed. Since these effects play a crucial role in the topological phase transition of TIs in the thin-film regime, we have carefully considered them in the present work.

III. THE PHASE TRANSITION IN ULTRATHIN Bi_2Se_3

A. Effect of thickness

The crossover from the three-dimensional topological insulator to its two-dimensional limit is accompanied by the emergence of an hybridization gap. Surface state wave functions overlap when sample thickness is comparable to the surface state penetration depth, and quantum tunneling between the upper and lower surface states opens such an hybridization gap (Δ_h) in these states. In Bi_2Se_3 the hybridization gap becomes considerable for samples of thickness below 7QL. The results of our calculations in that case, shown in Fig. 1(a), depict a topological phase transition from a TI with metallic surface states to a normal insulator (NI). The detection of the topological phase transformation shown in Fig. 1(c) can be made through surface state transport using the Landauer-Büttiker formalism, where we calculated the conductance G_{xx}. This conductance changes from 0 to $2e^2/h$ at the film thickness for which the hybridization gap vanishes. Once the system is in the thin film regime (2D), surface states have a gap, and the conductivity (G_{xx}) becomes zero due to the Fermi energy being inside the hybridization gap. However, as the thickness of the system increases, the gap between the surface states closes, and the system enters the three-dimensional phase. As a result, the Fermi energy cuts through the surface bands. Due to the band degeneracy in the system, two surface bands participate in conduction, resulting in a conductivity of $2e^2/h$.

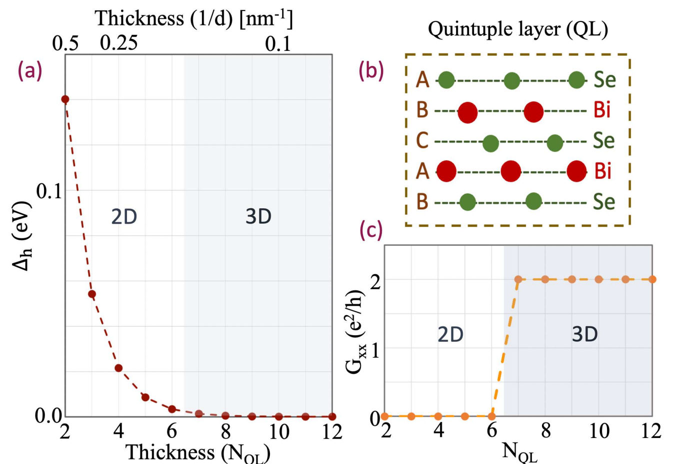

FIG. 1. (a) As the thickness of the TI is reduced, the wave functions of the surface states overlap, resulting in a hybridization gap (Δ_h) and a phase transition from the three-dimensional to the two-dimensional limit. (b) Schematic depiction of the Bi_2Se_3 unit cell, better known as the quintuple layer. (c) Conductance (G_{xx}) as a function of the film thickness (expressed as the number of quintuple layers, N_{QL}) for E_F = 5 meV, demonstrating the phase transition from the two-dimensional to the three-dimensional regime.

B. Effect of magnetization

In our model of a magnetic topological thin film, the magnetic impurities are distributed over the entire sample and not only on the surfaces. All magnetic impurities in the system have the same magnetization in terms of both direction and absolute value. The uniformity of magnetic moments is justified if only one kind of magnetic atoms (e.g. Cr) is used as substituents in the TI sites. The orientation of magnetic impurities can be aligned by an external magnetic field or by having mag-

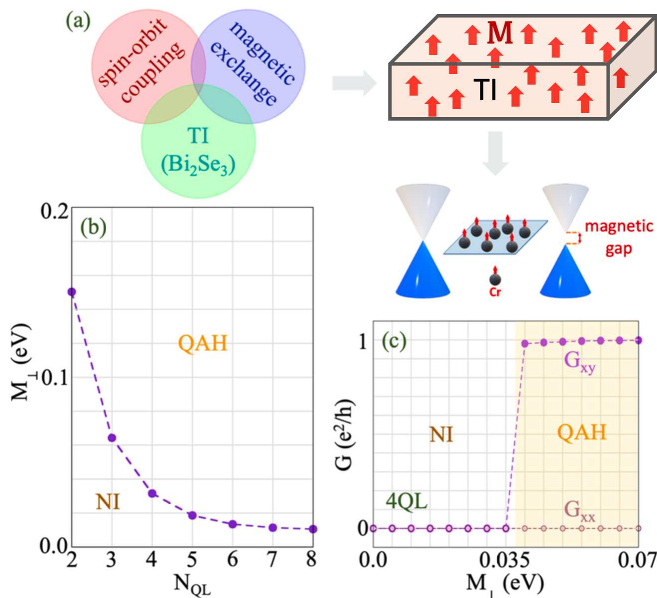

FIG. 2. (a) The presence of magnetization in TIs with a significant spin-orbit coupling yields diverse phenomena, such as the QAH effect. (b) Threshold out-of-plane magnetization for the transition from NI to QAH state in magnetic TI films of different thickness (N_{QL}). (c) Hall and longitudinal conductance as a function of out-of-plane magnetization M_z for a 4QL sample. Initially, Hall conductance and longitudinal conductance are both zero, and when M_z increases one observes G_{xy}=$1e^2/h$ and G_{xx}=0 (for $M_z \geq 0.04$ eV), indicating the QAH state.

netic layers proximitized to TI. Since the effect of in-plane magnetization in x and y directions is equivalent, we consider the magnetic momenta oriented in the $x - z$ plane. Finally we add the effect of magnetic impurities to the Hamiltonian solely via the exchange magnetization introduced in Eq. (4) in x and z directions. The larger magnetization then corresponds to a larger dopant concentration.

1. Out-of-plane magnetization

Magnetization induced in a TI by magnetic dopants or through the proximity effect breaks the TRS, and QAH can be identified by tuning the Fermi energy inside the exchange gap. In the absence of a magnetic field in a TI with strong spin-orbit coupling (SOC), the interaction between spin-orbit coupling and the exchange field caused by magnetization yields the QAH effect as shown schematically in Fig. 2(a).

Identifying QAH states in films thinner than 4QL is difficult since the hybridization gap rises as film thickness is decreased. The first observation of QAH effect was realized in a Cr-doped Bi_2Te_3 with a thickness of 5QL[8]. Fig. 2(b) shows the phase transition diagram from NI to QAH in terms of the thickness of Bi_2Se_3 and the

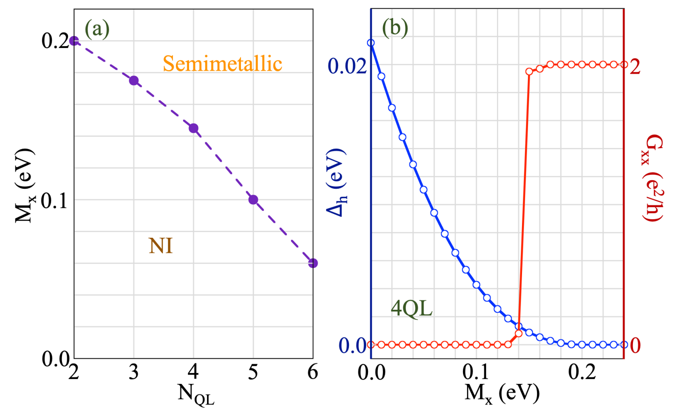

FIG. 3. (a) Threshold in-plane magnetization M_x for the phase transition from normal insulator (NI) to semimetallic state, for magnetically doped Bi_2Se_3 films of different thickness (N_{QL}). (b) Phase transition and behavior of the hybridization gap as a function of in-plane magnetization in a 4QL sample. The jump in longitudinal conductance G_{xx} signals a phase transition to a semimetallic state.

needed out-of-plane exchange magnetization. Hall conductance (G_{xy}) and longitudinal conductance (G_{xx}) are displayed in Fig. 2(c) for 4QL thick Bi_2Se_3. It should be noted that as the thickness of the TI is increased, due to an increase in parallel conduction channels generated by band bending and side surfaces, a deviation from the quantized value for Hall conductance can be observed, and detection of QAH states could be more complicated; thus, investigation of these states is typically performed in the ultra-thin film regime.

2. In-plane magnetization

Applying a magnetic field or magnetization in the in-plane direction to a three-dimensional TI could be described as a vector potential in the Hamiltonian; hence, the in-plane component of the surface state wave functions can be removed by using a gauge transformation. Due to the overlap of the top and bottom surface states, the ultra-thin film will have a non-zero diamagnetic response, and a gauge transformation can no longer remove the in-plane magnetization[40,41].

In ultra-thin TI, in-plane magnetization triggers a quantum phase transition from NI to a semimetal state. In-plane magnetization does not affect helical surface electrons. Through a gauge transformation, the in-plane component may cause Dirac cones to shift in momentum space. Due to quantum tunneling between surfaces in the ultra-thin film regime and since the phase factors on the top and bottom surface states are opposite, the gauge symmetry or chiral symmetry is broken, and the phase transition from NI to semimetal is possible[42]. This phase transition is equivalent to destroying two Dirac cones with identical spin winding numbers but with opposite signs.

Fig. 3(a) shows the threshold in-plane magnetization for the topological phase transition from NI to semimetallic state for ultra-thin Bi_2Se_3 samples with thicknesses ranging from 2QL to 6QL. Here we assumed the in-plane magnetization entirely in the x-direction. The longitudinal conductance (G_{xx}) calculations and the changes of hybridization gap for the 4QL-sample, which confirm this transition, are provided in panel (b) of Fig. 3. Applying in-plane magnetization to ultra-thin film TI decreases the hybridization gap to zero at some threshold magnetization M_x value, and the system enters the semimetallic phase. For the 4QL sample, the variation of the hybridization gap for different M_x values is also displayed. For M_x=0.15 eV, the jump in longitudinal conductance indicates that the sample enters its semimetal phase.

3. *Tilted magnetization*

The boundary condition scenarios of out-of-plane magnetization ($\theta = 0$) and in-plane magnetization ($\theta = \pi/2$) were investigated in the two last subsections. We showed that for an applied out-of-plane magnetization corresponding to the hybridization gap at $\theta = 0$, we might obtain QAH states. Still, for $\theta = \pi/2$, the surface state gap is minimized and eventually closed following semimetallic states. In this subsection, we will investigate the quantum phase transition using the magnetization rotation method, a feasible technique for manipulating the size and orientation of magnetization applied to ultra-thin films[2]. The magnetization rotates in the x-z plane, and θ determines the angle between the magnetization and the z-axis. A magnetic field applied externally may be used to control the magnetization direction. In practice, a Hall sensor measures the magnetization angle, and a standard lock-in method is applied to measure the resistance[39]. The analysis of topological phase transition in magnetic TI upon magnetization rotation has been performed in Ref. 39. Here, we explore magnetic TI in the ultra-thin film regime, highlight the relevance of the in-plane magnetization impact in this regime, and show that in-plane magnetization significantly influences the angle θ at which the phase transition from NI to QAH state occurs.

Ignoring the effect of in-plane magnetization on the surface states wave functions and only considering rotation in a way that controls the size of M_z as $M\cos\theta$ - such as in a 3D TI where the in-plane component can be cancelled using the gauge transformation and considering the top and bottom as two distinct surfaces - makes that the sole necessary condition for QAH states to occur is that $M\cos\theta > \Delta_h$. In such a case, the critical angle θ_c at which the phase transition from QAH to NI occurs for samples of thickness 4QL and 5QL at different M values is shown in the Fig. 4 (a-b), and indeed validates the threshold relation $\theta > \arccos(M/\Delta_h)$.

In the case of an ultra-thin film, where the wave functions of the surface states overlap, the influences of the phase factor of the in-plane component on the upper and lower surfaces are opposite to each other; therefore, it is impossible to use a unitary transformation to eliminate the in-plane component. Therefore, we consider magnetization as M_x, $M_z = (M\sin\theta, M\cos\theta)$ and investigate how it alters the quantum phase transition from QAH to NI in 4QL and 5QL samples. As shown in the Fig. 4 (c-d), the critical angle θ_c, for which we induce a quantum phase transition from QAH to NI, increases with M and eventually reaches a maximum value of $\theta \approx 11\pi/40$. When the angle θ is larger than $11\pi/40$, the system is in the NI phase because the in-plane magnetization component becomes dominant.

C. Effect of strain

Applying strain to a thin-film TI, either stemming from its lattice mismatch with the substrate or as a consequence of an applied force, is an established method for tailoring the TI properties[41]. One modifies both the TI's physical properties and band structure by applying strain, particularly its bulk and hybridization gaps. As illustrated in Ref. 43, one can adjust these gaps to modify the magnetization threshold for achieving QAH states. Here, we define out-of-plane uniaxial strain as $\epsilon_\perp = \frac{c-c_0}{c_0}$, where c_0 is the lattice constant in the z-direction of the unstrained structure. The Poisson ratio describes the relationship between the biaxial in-plane strain and the uniaxial out-of-plane strain as follows:

$$\frac{\epsilon_\perp}{\epsilon_\parallel} = -\frac{2\nu}{1-\nu}, \tag{6}$$

where $\nu = 0.27$ for Bi_2Se_3[44,45]. The strain changes the bond length and bond angles, thereby altering the Hamiltonian parameters. According to the system symmetries, the following terms are added to the system hopping in that case:

$$E_0 \;\rightarrow (E_0 + \tilde{E}_1\epsilon_{zz} + \tilde{E}_2\epsilon_+)\sigma_z \otimes \tau_0, \tag{7}$$

$$T_\alpha \;\rightarrow \tilde{A}_\alpha \epsilon_\alpha\, \sigma_x \otimes \vec{\sigma} \cdot \vec{n}_\alpha. \tag{8}$$

In this work, we employ the values of these parameters taken from Ref. 46. The phase transition from QAH to NI under uniaxial out-of-plane strain and the dependence of the critical tilt angle and magnetization value for this phase transition as a function of applied strain are shown in the Fig. 4 (c-d), for films of thickness 4QL and 5QL. Note that the indicated values of the vertical strain $\epsilon_\perp$ are also accompanied by the in-plane strain $\epsilon_\parallel$ given by Eq. (6). The results clearly show that strain can indeed be used to broadly control the phase transition. Nevertheless, the maximum value of the magnetization tilt angle $\theta \approx 11\pi/40$ above which the system enters the NI phase cannot be increased.

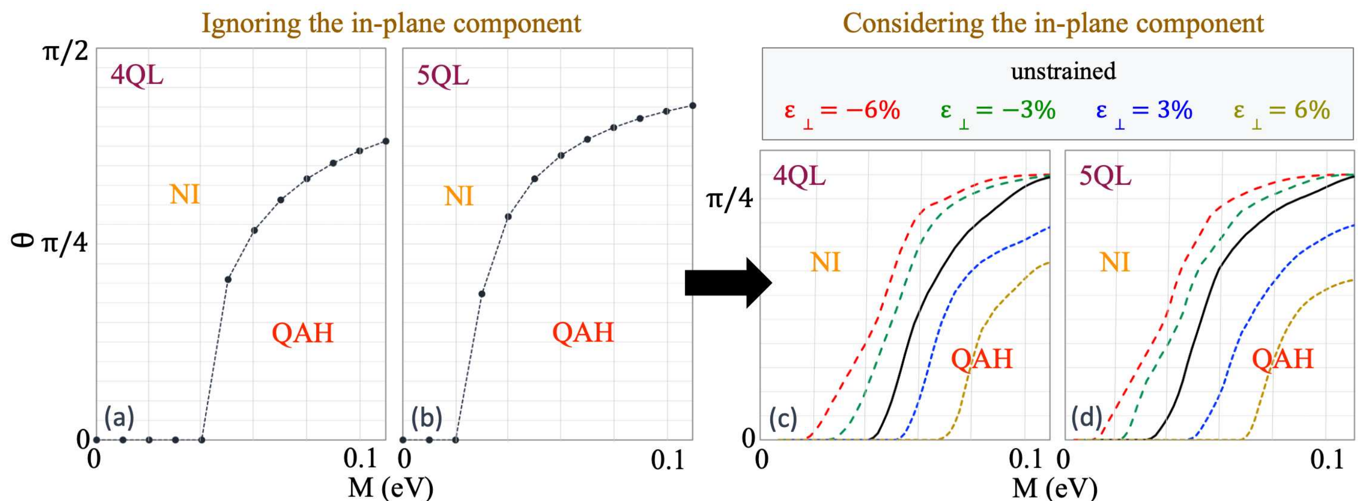

FIG. 4. (a-b) Tilt angle θ at which the phase transition from QAH to NI state occurs, as a function of applied magnetization M, for (a) 4QL and (b) 5QL samples. The tilting is exclusively considered to control the magnitude of orthogonal (M_z) magnetization component, and the in-plane component is ignored. (c-d) NI-QAH phase diagram as a function of magnetization and its tilt angle, now considering the effect of in-plane magnetization, also in presence of strain, for samples of thickness (c) 4QL and (d) 5QL. For a given magnetization, the threshold angle θ_c for QAH to NI transition can be broadly tuned by strain, but the overall maximal value of θ_c will not rise since for large angles the in-plane magnetization is the determining factor.

D. Effect of vertical gating

Since the vdW interaction between the Bi_2Se_3 layers is weak and the spacing between the layers is sensitive to the environment[21], the substrate may have a considerable effect on the properties of the thin-film TI. As the film is grown on a substrate, inversion symmetry is broken in the out-of-plane direction, analogously to when a vertical electric field is applied to the TI. Band bending generated by the substrate (or more generally, the separate environments for the top and bottom surfaces) may enhance the breaking of structural inversion symmetry in the film, resulting in Rashba-type spin splitting[1]. To capture this effect, one considers an effective electric potential V, perpendicular to the surface, in order to add the substrate effect to the model (as depicted in Fig. 5).

The exploration of QAH states for the Bi_2Se_3 family typically focuses on thicknesses between 4QL and 6QL. For thicknesses below this range, the overlap of surface states causes a significant gap, and the transition to QAH states is practically impossible. Band-bending and the side-surface effect hamper the formation of QAH states for thicknesses above this range[29,47,48]. The threshold values of M_z at which the topological quantum phase transition from NI to QAH occurs in 4QL and 5QL samples under different values of V are shown in Fig. 5. With increasing electric potential V in the ultra-thin film regime, the conduction states on one surface increasingly overlap with the valence band states on the opposite surface, and the sample transits from a QAH state with a Chern number of one to an NI state with a Chern number of zero. An electric field can thus induce a phase transition from QAH to NI, but a phase transition from NI to QAH is inconceivable[49].

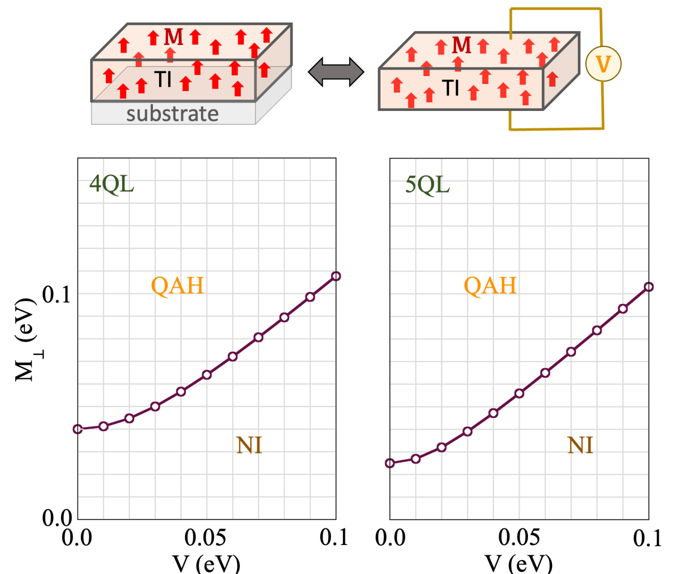

FIG. 5. Threshold magnetization for the phase transition from NI to QAH state for samples of thickness 4QL and 5QL, as a function of the vertical gate potential V. Increasing V raises the QAH gap in the thin film and increases the threshold value for the transition to QAH state.

IV. SUMMARY AND CONCLUSIONS

In condensed matter physics, description of topological phases of materials and quantum phase transitions

under different conditions belongs among the key fundamental research questions. In this work, we considered such phases and transitions in ultra-thin films of magnetically doped Bi_2Se_3, which can be successfully grown experimentally, with well controllable properties such as choice and concentration of dopants.

Starting from a real-space tight-binding model for pristine Bi_2Se_3, we first validated the crossover from a three-dimensional to a two-dimensional limit below the film thickness of 6QL. We then proceeded to investigate ultra-thin magnetic TI film, for different magnetization orientation of its uniformly distributed dopants, revealing that the TRS is broken by adding out-of-plane magnetization to the TI. A phase transition from NI to QAH happens when the ferromagnetic magnetization gap is proportional to the hybridization gap. Commonly, 4QL-6QL samples are used to realize the QAH states since the hybridization gap becomes substantial below 4QL thickness, and side surface effects become considerable above 6QL thickness. Subsequently, the impact of in-plane magnetization was analyzed, and it was shown that this magnetization component can trigger a transition from NI to semimetallic states in ultra-thin films. Such phase transitions can be captured experimentally through electronic transport measurements. Therefore, we validated the observed transitions by the accompanying transport calculations using the Landauer-Büttiker formalism.

As a next step, we examined the effect of tilting the magnetization as a practical experimental method for control, which mixes the effects of different magnetization components in a nontrivial manner. We demonstrated that the in-plane component plays an important role that cannot be eliminated with a unitary transformation, unlike in the case of three-dimensional TI. Using magnetization tilt in the $x - z$ plane (θ is the angle of magnetization with respect to the z-axis) of an ultra-thin film, we revealed that the critical tilt angle at which the transition from QAH to NI takes place increases with magnetization M, but converges to the maximum value $\theta_c \approx 11\pi/40$ since the in-plane magnetization takes the dominant role at large angles. Strain can be employed to broadly tune the magnetization and tilt angle threshold for the quantum phase transition, as it controls the hybridization gap. Finally, we showed that in the presence of a substrate effect and/or applied gating, the threshold value of M_z for the quantum transition from NI to QAH increases. Taken together, our results provide a useful platform for practical tunability of topological phase transitions in thin-film TIs, that may find its further use in both fundamental studies and device concepts.

ACKNOWLEDGMENTS

This research was supported by the Research Foundation-Flanders (FWO-Vlaanderen), the Special Research Funds (BOF) of the University of Antwerp, the Isfahan University of Technology, and the FWO-FNRS EoS-ShapeME project.

* milorad.milosevic@uantwerpen.be

[1] Y. Zhang, K. He, C.-Z. Chang, C.-L. Song, L.-L. Wang, X. Chen, J.-F. Jia, Z. Fang, X. Dai, W.-Y. Shan, *et al.*, Nature Physics **6**, 584 (2010).
[2] X. Kou, L. Pan, J. Wang, Y. Fan, E. S. Choi, W.-L. Lee, T. Nie, K. Murata, Q. Shao, S.-C. Zhang, *et al.*, Nature Communications **6**, 8474 (2015).
[3] C.-Z. Chang, W. Zhao, J. Li, J. Jain, C. Liu, J. S. Moodera, and M. H. Chan, Physical Review Letters **117**, 126802 (2016).
[4] J. Wang, B. Lian, and S.-C. Zhang, Physica Scripta **2015**, 014003 (2015).
[5] K. Yasuda, *Emergent Transport Properties of Magnetic Topological Insulator Heterostructures* (Springer Nature, 2020).
[6] J. Wang and S.-C. Zhang, Nature Materials **16**, 1062 (2017).
[7] F. D. M. Haldane, Physical review letters **61**, 2015 (1988).
[8] C.-Z. Chang, J. Zhang, X. Feng, J. Shen, Z. Zhang, M. Guo, K. Li, Y. Ou, P. Wei, L.-L. Wang, *et al.*, Science **340**, 167 (2013).
[9] X.-G. Wen, Science **363**, 3099 (2019).
[10] M. J. Gilbert, Communications Physics **4**, 1 (2021).
[11] L. Fu, C. L. Kane, and E. J. Mele, Physical Review Letters **98**, 106803 (2007).
[12] D. Hsieh, Y. Xia, D. Qian, L. Wray, F. Meier, J. Osterwalder, L. Patthey, J. G. Checkelsky, N. Ong, A. V. Fedorov, *et al.*, Nature **460**, 1101 (2009).
[13] H. Zhang, C.-X. Liu, X.-L. Qi, X. Dai, Z. Fang, and S.-C. Zhang, Nature Physics **5**, 438 (2009).
[14] Y. Xia, D. Qian, D. Hsieh, L. Wray, A. Pal, H. Lin, A. Bansil, D. Grauer, Y. S. Hor, R. J. Cava, *et al.*, Nature Physics **5**, 398 (2009).
[15] Y. Hor, A. Richardella, P. Roushan, Y. Xia, J. Checkelsky, A. Yazdani, M. Hasan, N. Ong, and R. Cava, Physical Review B **79**, 195208 (2009).
[16] A. Taskin, S. Sasaki, K. Segawa, and Y. Ando, Physical Review Letters **109**, 066803 (2012).
[17] L. He, F. Xiu, X. Yu, M. Teague, W. Jiang, Y. Fan, X. Kou, M. Lang, Y. Wang, G. Huang, *et al.*, Nano Letters **12**, 1486 (2012).
[18] X.-L. Qi and S.-C. Zhang, Reviews of Modern Physics **83**, 1057 (2011).
[19] S. Li, H. M. Soliman, J. Zhou, M. S. Toprak, M. Muhammed, D. Platzek, P. Ziolkowski, and E. Müller, Chemistry of Materials **20**, 4403 (2008).
[20] L. He, X. Kou, and K. L. Wang, Physica Status Solidi (Rapid Research Letters) **7**, 50 (2013).
[21] C.-X. Liu, H. Zhang, B. Yan, X.-L. Qi, T. Frauenheim, X. Dai, Z. Fang, and S.-C. Zhang, Physical Review B **81**, 041307 (2010).
[22] Y. Tokura, K. Yasuda, and A. Tsukazaki, Nature Reviews Physics **1**, 126 (2019).

[23] C.-X. Liu, S.-C. Zhang, and X.-L. Qi, Annual Review of Condensed Matter Physics **7**, 301 (2016).
[24] I. Lee, C. K. Kim, J. Lee, S. J. Billinge, R. Zhong, J. A. Schneeloch, T. Liu, T. Valla, J. M. Tranquada, G. Gu, *et al.*, Proceedings of the National Academy of Sciences **112**, 1316 (2015).
[25] Y. Chen, J.-H. Chu, J. Analytis, Z. Liu, K. Igarashi, H.-H. Kuo, X. Qi, S.-K. Mo, R. Moore, D. Lu, *et al.*, Science **329**, 659 (2010).
[26] R. Yu, W. Zhang, H.-J. Zhang, S.-C. Zhang, X. Dai, and Z. Fang, Science **329**, 61 (2010).
[27] J. Zhang, C.-Z. Chang, P. Tang, Z. Zhang, X. Feng, K. Li, L.-l. Wang, X. Chen, C. Liu, W. Duan, *et al.*, Science **339**, 1582 (2013).
[28] K. Nomura and N. Nagaosa, Physical Review Letters **106**, 166802 (2011).
[29] K. He, Y. Wang, and Q.-K. Xue, Annual Review of Condensed Matter Physics **9**, 329 (2018).
[30] S. Bhattacharyya, G. Akhgar, M. Gebert, J. Karel, M. T. Edmonds, and M. S. Fuhrer, Advanced Materials **33**, 2007795 (2021).
[31] R. S. Mong, A. M. Essin, and J. E. Moore, Physical Review B **81**, 245209 (2010).
[32] L. Bao, W. Wang, N. Meyer, Y. Liu, C. Zhang, K. Wang, P. Ai, and F. Xiu, Scientific Reports **3**, 2391 (2013).
[33] A. Pertsova and C. M. Canali, New Journal of Physics **16**, 063022 (2014).
[34] C.-X. Liu, X.-L. Qi, H. Zhang, X. Dai, Z. Fang, and S.-C. Zhang, Physical Review B **82**, 045122 (2010).
[35] L. Fu and C. L. Kane, Physical Review B **76**, 045302 (2007).
[36] D. Hsieh, Y. Xia, D. Qian, L. Wray, F. Meier, J. Dil, J. Osterwalder, L. Patthey, A. Fedorov, H. Lin, *et al.*, Physical Review Letters **103**, 146401 (2009).
[37] M. Shafiei, F. Fazileh, F. M. Peeters, and M. V. Milošević, Physical Review B **109**, 045129 (2024).
[38] S. Datta, *Electronic transport in mesoscopic systems* (Cambridge University Press, 1997).
[39] M. Kawamura, M. Mogi, R. Yoshimi, A. Tsukazaki, Y. Kozuka, K. S. Takahashi, M. Kawasaki, and Y. Tokura, Physical Review B **98**, 140404 (2018).
[40] A. Zyuzin, M. Hook, and A. a. Burkov, Physical Review B **83**, 245428 (2011).
[41] M. Shafiei, F. Fazileh, F. M. Peeters, and M. V. Milošević, Physical Review B **106**, 035119 (2022).
[42] Y. Xu, G. Jiang, I. Miotkowski, R. R. Biswas, and Y. P. Chen, Physical Review Letters **123**, 207701 (2019).
[43] M. Shafiei, F. Fazileh, F. M. Peeters, and M. V. Milošević, Physical Review B **107**, 195119 (2023).
[44] H. Aramberri and M. C. Muñoz, Physical Review B **95**, 205422 (2017).
[45] X. Gao, M. Zhou, Y. Cheng, and G. Ji, Philosophical Magazine **96**, 208 (2016).
[46] S. M. Young, S. Chowdhury, E. J. Walter, E. J. Mele, C. L. Kane, and A. M. Rappe, Phys. Rev. B **84**, 085106 (2011).
[47] J. Checkelsky, R. Yoshimi, A. Tsukazaki, K. Takahashi, Y. Kozuka, J. Falson, M. Kawasaki, and Y. Tokura, Nature Physics **10**, 731 (2014).
[48] X. Kou, S.-T. Guo, Y. Fan, L. Pan, M. Lang, Y. Jiang, Q. Shao, T. Nie, K. Murata, J. Tang, *et al.*, Physical Review Letters **113**, 137201 (2014).
[49] C. Lei and A. H. MacDonald, Physical Review Materials **5**, L051201 (2021).